Severe Plastic Deformation by Equal Channel Angular Pressing and Rolling: The Influence of the Deformation Path on Strain Distribution

Andrea M. Kliauga,* Vitor L. Sordi, Natalia S. De Vincentis, Raúl E. Bolmaro, Norbert Schell, and Heinz-Günter Brokmeier

The present work compares two deformation techniques, rolling and Equal Channel Angular pressing (ECAP), and the response offered by three different materials that differ in Stacking Fault Energy (SFE): AA1010 Al, commercially pure Cu, and an austenitic stainless steel. The objective of this investigation is to study the effect of each deformation mode on tensile behavior, deformation mechanism, texture, and microstructure and to establish the influence of the stacking fault energy on said effects. The results show that the different strain paths of ECAP and rolling do not affect the strength, but rolling leads to an accentuated texture and thus to elastic and plastic anisotropy. This finding has practical relevance for micro manufacturing techniques. Furthermore, it is observed that lower SFE results in smaller domain size and higher dislocation density, which are microstructural details related to strength and to the work hardening capacity. Finally, both techniques are able to produce a high amount of high angle grain boundaries, a feature that characterizes refined microstructures. These processes operate at different strain rates; thus, in low SFE materials, a more effective grain fragmentation by deformation-induced twins is observed after the ECAP process.

1. Introduction

Among the processes devised to obtain grain refinement in metals and alloys, those that are designated as Severe Plastic Deformation (SPD) are very effective. They are characterized by an important strength enhancement due to the Hall–Petch effect, and this can be accomplished by a number of different techniques, such as Equal Channel Angular Pressing (ECAP), conventional rolling, accumulated roll bonding and high-pressure torsion, among others. With said techniques, a workpiece is subjected to cold or warm processing to very large strains. Rolling is also used as a complementary process to produce sheet material after ECAP.[1,2] Therefore, it is interesting to compare the strength obtained by cold rolling with that obtained by ECAP processing. In this respect, Horita et al.[3] working with Al alloys, observed only a very small difference in strength between them. A similar conclusion was found by Sarma et al.[4] by comparing room temperature rolling with ECAP processing of Al and Cu and their alloys.

It is well known that, besides microstructural features such as grain size (scale of tens of nanometers), the properties induced in a material that is plastically deformed by either ECAP or rolling are highly dependent on the degree of deformation and accumulated deformation energy. The structural defects thus formed operate by restricting the mobility of companion defects; therefore, it is important to follow the development of misorientation distribution and of crystallographic texture.

The most suitable experimental technique for the structural characterization of heavily deformed materials is X-ray diffraction because the resulting diffraction profile is affected by the defects.[5] Thus, analysis of the broadening of the diffraction peaks allows for quantitative description of both dislocation and stacking fault densities as well as crystallite sizes. The first micromechanical model employed for said calculation was the Williamson-Hall (W-H) method,[5] later modified by Warren[5] and Ungár.[6–9] The advantage of the X-ray diffraction technique is its capability to obtain information about volumes on the order of a few hundred micrometers, and the resolution of the

Prof. Dr. A.M. Kliauga
Materials Engineering Department, São Carlos
Federal University, Rodovia Washington Luiz km 235, 13565-905 São Carlos, Brazil
E-mail: kliauga@ufscar.br

Prof. Dr. V. L. Sordi
Materials Engineering Department, São Carlos
Federal University, São Carlos, Brazil

Dr. N. S. De Vincentis, Prof. Dr. R.E. Bolmaro
Instituto de Física Rosario — FCEIA-UNR-CONICET, Rosario, Argentina

Dr. N. Schell, Prof. Dr. H.-G. Brokmeier
InstitutfürWerkstoffkunde und Werkstofftechnik,
TU Clausthal, Clausthal, Germany

Dr. N. Schell, Prof. Dr. H.-G. Brokmeier
Helmholtz-ZentrumGeesthacht, GEMS
Outstation, Hamburg, Germany

The ORCID identification number(s) for the author(s) of this article can be found under https://doi.org/10.1002/adem.201700055.

Table 1. Chemical composition of the materials (in wt%) used in this work.

	Ni	Cr	Mn	Mg	Mo	Zn	Si	Cu	C	P	S	Al	Fe
F138	14.31	17.33	1.79	–	2.79	–	0.3	0.09	0.015	0.022	0.002	–	63.351
Cu −C1100	–	–	–	–	–	–	–	99.9	–	–	–	–	–
Al −AA1050	–	–	0.003	0.003	–	0.002	0.081	0.012	–	–	–	99,7	0.185

equipment is of the utmost importance because it defines its capability for detecting the misorientation between domains, which, in turn, depends on the machine peak broadening, that is, the angular dispersion of the incident radiation. Whereas the dispersion is approximately one tenth of a degree for a conventional diffractometer, for a synchrotron light facility, this characteristic is one order of magnitude smaller, resulting in much better resolution.

One of the purposes of this work is to compare deformation by rolling and ECAP in terms of the resulting accumulated strain, effective grain refinement, and texture. Hence, optical scanning electron microscopy and X-ray diffraction techniques were employed to evaluate the microstructural changes in three fcc materials: Al, Cu, and an austenitic stainless steel. The results have practical importance in forming technologies, such as deep drawing and micro manufacturing because texture and grain size have a profound influence on the feasibility and quality of said techniques. Additionally, the literature shows many instance of the sequence ECAP plus rolling, but a more complete description of the effect that such sequence has on the crystallographic alignment is still lacking.

2. Experimental Section

Table 1 gives the composition of the materials employed in the present study: commercially pure Cu, Al (AA1050) and F138 stainless steel, whose composition is close to that of 316L steel. These materials were chosen because they represent a range of stacking fault energy (SFE) values. Deformation was produced by conventional rolling at room temperature in several passes up to a von Mises strain of 2.0 and by ECAP using a die with an internal angle of 120° up to a von Mises strain equal to 5.6 (each pass produces a strain of 0.7). Route A utilizes an ECAP variant, in which there is no billet rotation around its longitudinal axis between each pass. Some Al billets, which were ECAP deformed by one and four passes resulting in equivalent strains of 2.1 and 4.2, respectively, were further subjected to rolling up to a thickness reduction of 70%. In these latter experiments, rolling was performed along the extrusion direction.

The sample reference axes for ECAP were chosen, as shown in **Figure 1**, while for the rolled materials, the conventional notation was employed, that is, RD denotes the rolling direction, TD the transverse, and ND the normal direction. The ECAP billet cross-section and length were equal to 14 × 14 mm² and 70 mm, respectively.

For samples in the annealed conditions, tensile tests at room temperature were performed in an INSTRON universal testing machine using specimens with a circular cross section, which had a diameter of 5 mm and gauge length of 25 mm. For all processed samples, miniature tensile specimens with a gauge length of 7 mm and 3 × 2 mm² cross-section area were extracted at the midpoint of the billet and as far as possible from its surface, maintaining their axis parallel to the pressing and rolling directions. All tensile tests were performed at room temperature and at a nominal strain rate of $1 \times 10^{-3}\,s^{-1}$ with the elongation monitored by optical extensometry. Vickers hardness measurements were performed on a Future Tech microhardness tester under a load of 300 g maintained over 10 s.

Optical and scanning electron microscopy observations of the microstructure were performed on a plane perpendicular to the ECAP pressing direction and the transverse direction (TD) for the rolled samples. The samples were prepared by conventional techniques followed by a final polishing in 0.05 μm colloidal silica. EBSD analysis was carried out, employing an FEI Quanta 200 scanning electron microscope (SEM) equipped with automatic OIM and TSL-EDAX software located at IFIR-Argentina. TEM samples were prepared by electrolytic etching (30% HNO_3 in methanol, 5 and 20 V for Cu and Al, respectively; 20% $HClO_4$ in ethanol, 30V for the F138 steel) and observed in a CM120 FEI microscope located at UFSCar, Brazil.

The diffraction experiments in the Synchrotron National Laboratory − LNLS (Campinas, Brazil) were performed in reflection geometry at an X-ray beamline with a radiation wavelength of 0.12678 nm and angular dispersion of ≈0.1°. At the Helmholtz-Zentrum Geesthacht, GEMS Outstation, the analysis was carried out in transmission geometry with a 0.01427 nm wavelength and ≈0.01° angular divergence. A translation-rotation stage was used to obtain 37 Debye-Scherrer image plates in a Mar345 solid-state area detector every 5° (180° span around vertical axes), gathering information on all orientation planes employing a single measurement. Background subtraction was performed by using, alternatively, Si or LaB6 powder standards. The instrumental contribution was subtracted from the peak breadths according to Cagliotti's equation.[10] On the diffractograms, peak broadening was analyzed by the Williamson-Hall (W-H) method[11] and modified by Ungár[6–9,12] and Warren[5] (MW-H) using the following equation:

$$\frac{\text{Breath } \cos\theta}{\lambda} - \beta W_g = \frac{1}{d} + \left(\frac{\pi M^2 b^2}{2}\right)\rho^{1/2}K^2C \qquad (1)$$
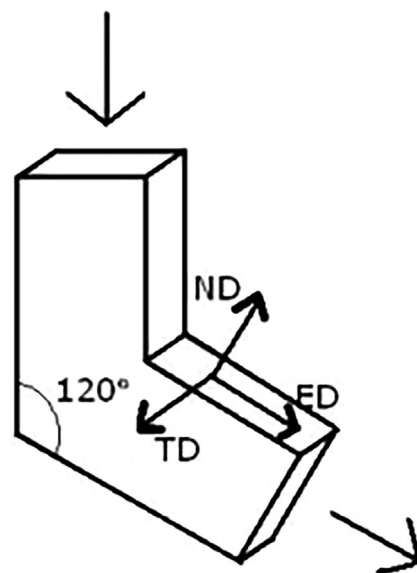

Figure 1. Schematic representation of the sample reference system: ED, extrusion direction; ND, normal direction; TD, transverse direction.
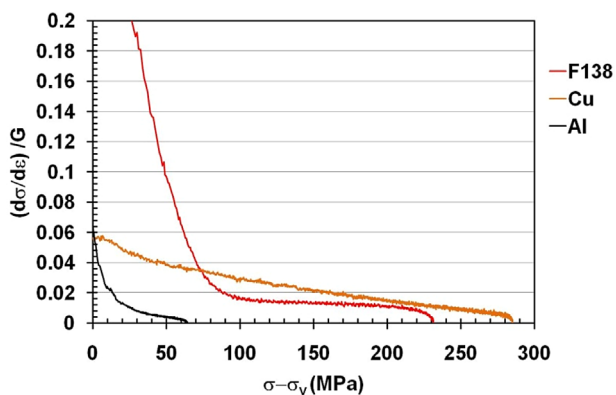
Figure 2. Work hardening rate ($d\sigma/d\varepsilon$) normalized by the shear modulus G calculated from tensile test data of the annealed materials.

where Θ is the Bragg angle, λ the radiation wavelength, β the twin density, W_g the Warren constants related to the stacking faults, d the diffraction domain size, ρ the dislocation density, and b the Burger's vector. M is a constant related to the cut-off radius of dislocations (which is smaller for more compact arrays); C is the average contrast factor of dislocations, and K is equal to $2\sin(\theta)/\lambda$.

3. Results and Discussion

There are two deformation mechanisms for metals that lead to the formation of ultra-fine grain structures by SPD: dislocation glide and twinning. In the majority of crystal structures, the latter forms more readily as the temperature of deformation is decreased or the rate of plastic deformation is increased. Although slip is the preferred mode of deformation for most metals over a wide range of temperatures, when the temperature is very low, the stress required for twinning can become lower than that for slip.[13] Another important factor for the prevalence of either deformation mechanism is the SFE of the material: Al has a high SFE of approximately $166 \, mJ \, m^{-2}$, that of Cu is close to $80 \, mJ \, m^{-2}$, and F138 SS has a value between 30 and $40 \, mJ \, m^{-2}$. Finally, the nucleation of mechanical twins is critically dependent upon the grain size, the amount of pre-strain, and the stress conditions of the material prior to its deformation.

Figure 2 is a Kocks-Mecking (K-M) plot, showing the strain hardening rate of the three samples given in terms of ($d\sigma/d\epsilon$) normalized by the shear modulus G; σ and σ_y are a given stress and the yield stress, respectively. The F138 steel exhibits a plateau, indicating a constant strain-hardening rate, a feature that characterizes a twin-mediated deformation, whereas in the Cu and Al samples, said plateau is absent. These results can be compared with the those shown by El-Danaf, obtained on Cu, brass, and austenitic stainless steels[14] and with those of Steinmetz et al.[15] also on austenitic steel grades. Both investigations also observed a plateau on the K-M plots. For austenitic stainless steels, twinning is reported to occur at SFE within the range 18–45 mJ m^{-2}[15–17]; martensitic transformation can be favored by SFE lower than 18 mJ m^{-2}, whereas dislocation glide would be the prevailing deformation mechanism when SFE exceeds 45 mJ m^{-2}.

Figure 3 shows the microstructures of Al, Cu, and F138 stainless steel after four ECAP passes and rolling to 70% thickness reduction, respectively. It can be seen that the density of defects changes with the materials SFE; thus, Al exhibits elongated grains with a highly recovered sub-grain structure, a characteristic of its high SFE. For Cu and F138 steel, a high dislocation density, small dislocation cell size, and no deformation twins were observed in the former, whereas the latter was characterized by extensive twinning. It must be noted that the microstructural observation confirms the findings expressed in Figure 2, that is, the prevalence of twinning as the deformation mode for the low SE material. For Al and Cu, the structural refinement appears to be more effective in the rolled samples than in those that were ECAP processed in route A, and a detailed quantification of the microstructural characteristics produced by either deformation technique will be given when discussing the X-ray diffraction results.
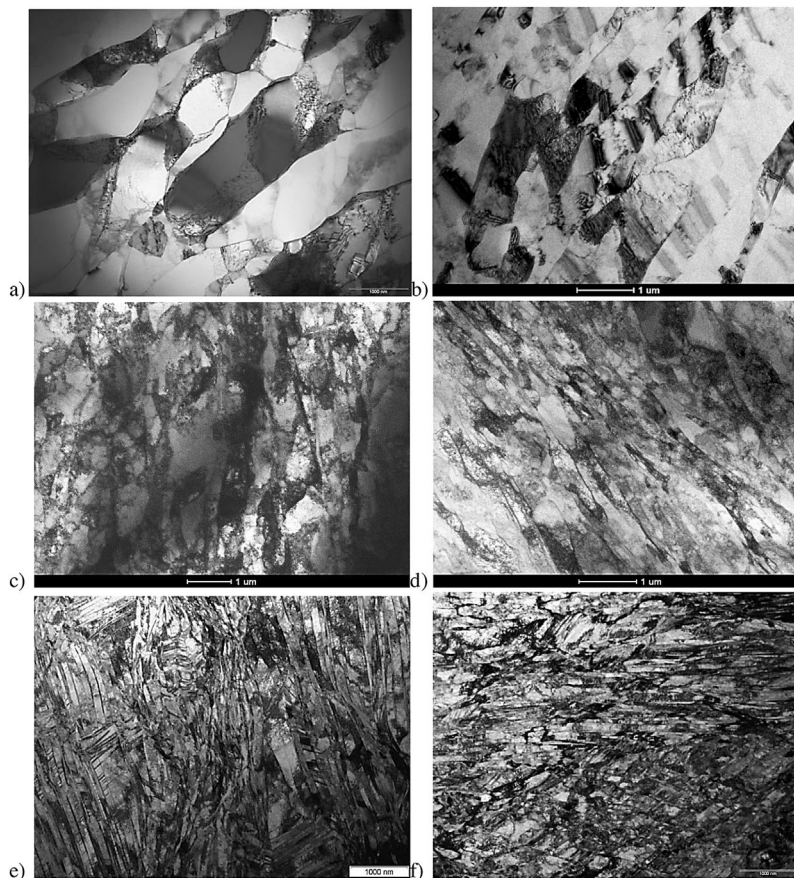

Figure 3. Transmission electron microscopy of Al a, b), Cu c, d), and F138 SS e, f) after four ECAP passes and rolling to 70% thickness reduction, respectively.

Table 2. Hardness and tensile properties of the samples after rolling and ECAP processing: ε_{eq}, equivalent strain applied in the process; HV, vickers hardness; σ_y, yield stress; ε_u, uniform elongation; ε_t, total elongation.

Material	Condition/Process	Sample	ε_{eq}	Hardness [HV]	σ_y[MPa]	ε_u[%]	ε_t[%]
AA1050	Annealed	A	0	17.1	45	10	70
	Rolling	R30	0.4	35.6	85		29
		R50	0.8	38.7	110		19
		R1.4	1.4	43.5	128	2.2	20
		R2.5	2.7	47.5	145		20
	ECAP	E0.7	0.55	43.3	120	1.2	24
		E1.7	1.05	49.8	128	2.0	26
		E2.1	1.55	50.3	145	1.9	26
		E2.8	2.05	49.7	150	2.0	27
		E5.6	4.05	52.2	165	2.0	27
	ECAP + rolling	E0.7R1.4	2.9	50.3	144	2.4	22
		E2.8R1.4	4.2	51.1	160	3.1	23
Copper	annealed	A	0	50	43	40	70
	ECAP	E0.7	0.55	130	319	3.3	45
		E1.4	1.05	127	331	2.5	28
		E2.8	1.55	136.5	385	2,5	34
		E5.6	3	136	380	2.5	27
	rolling	R0.5	0.5		331		
		R2.5	2.5		405		
F138	annealed	A	0.55	130	550	23	30
	ECAP	E0.7	1.05	321	889	2.8	36
		E1.4	1.55	339	1055	2.8	28
		E2.8	2.05	473	1140	4.2	26
	rolling	R1.4	1.4	374	1100	3.5	32

The HV hardness and the tensile properties of the deformed samples are summarized in **Table 2**. For all samples, the yield stress saturates after an equivalent strain of 3–4; the uniform elongation (ε_u) is drastically reduced, while the total elongation (ε_t) is close to one third of that for annealed samples, except for the steel, which is left unchanged. It must be noted that miniature tensile samples were employed when testing the SPD samples, whose elongation is then overestimated. However, ϵ_u, a parameter most relevant to the design, is very small, thus minimizing the error.

The behavior of the uniform elongation (and total elongation as well for Al and Cu) is a consequence of the strain localization, which, in turn, is a result of grain refinement below 2 μm, a feature that contributes to inhomogeneous yields.[18] This phenomenon is caused by the lack of initial mobile dislocations because for grains of such reduced size, the dislocations are mainly associated with the boundaries.

It is common knowledge that yield strength and hardness are connected with the dislocation density and grain size; thus, by considering the von Mises equivalent strain, it should be possible to fit these mechanical properties to a flow rule criterion independent of the deformation mode.[19] In this respect, the present results are reasonably well described by the constitutive relationship proposed by Chinh et al., relating strain (ε) and tensile strength,[20]

$$\sigma = \sigma_0 + \sigma_1 \left[1 - \exp\left[\left(-\frac{\varepsilon}{\varepsilon_c} \right)^n \right] \right] \tag{2}$$

where σ_0 is the yield strength of the annealed material and σ_1 is the difference between the saturation stress (σ_{sat}) and σ_0. The value of the macroscopic parameter ε_c depends on the thermally activated dislocation trapping and annihilation mechanisms, and n corresponds to the strain-hardening exponent in the conventional Hollomon power-law relationship.

Figure 4 shows the experimental σ_y data for AA1050 Al, Cu, and F138 together with literature data[20–37] relative to the von Mises strain. This is superimposed on the flow relationship given by Equation 2. For the F138 stainless steel, there is less information in the literature on its work hardening rate; thus, a comparison was made with AISI 316L steel, which has a similar composition. Csanádi et al.[22] calculated fitting parameters for some fcc alloys; these were employed here for drawing the Cu and Al theoretical curves. For the F138 stainless steel, the ε_c and n were calculated to fit the experimental data, and all adjustment constants are given in **Table 3**.

Figure 4 shows a good fit between the theoretical curve and experimental data for Cu and Al. Cu saturates hardness at lower
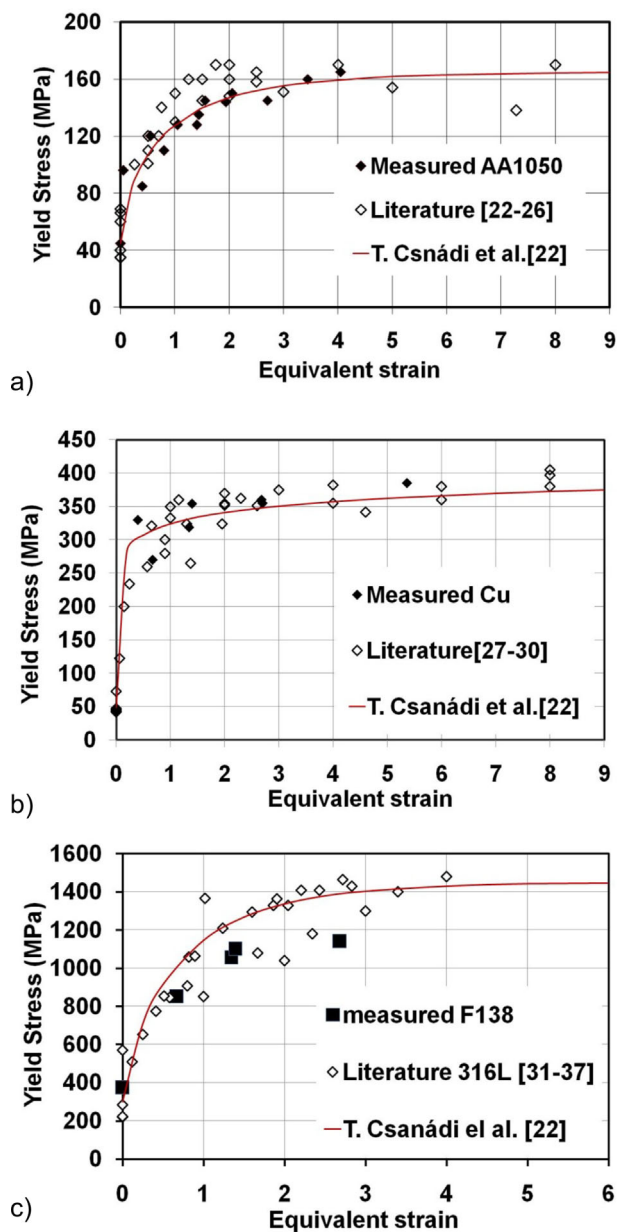
**ADVANCED
SCIENCE NEWS**

www.advancedsciencenews.com

**ADVANCED
ENGINEERING
MATERIALS**

www.aem-journal.com

Figure 4. Yield stress as a function of equivalent strain for a) Al, b) Cu, and c) F138. Data from the present study (■) and from the literature[15–37] (◇) and a theoretical curve drawn using the flow equation with the fitting parameters suggested by Csanádi et al.[22]

strains, and according to a number of investigations,[28–30] it takes longer to build up grains by SPD (in comparison to Al, twice as much strain is required to obtain high-angle grain boundaries (HAGBs) because its recovery process is slower. Conversely, Figure 4c shows that the F138 steel has a lower hardening saturation level compared with that in the literature because it does not undergo martensitic transformation as the 316L steel, which was used to draw the flow curve.

Data show that different processing methods (ECAP, rolling, accumulative roll bonding, high-pressure torsion, rotary swaging, wire drawing) give very similar tensile strengths, even in

cases where the same material is subjected to different strain paths and consequently develops different microstructures. In plastic deformation processes, with increasing strain, the average dislocation density increases while the individual crystallite size becomes smaller. In the three materials studied here, these two quantities reach their saturation at an imposed strain value of approximately 3–4.

However, this has important consequences on the microstructure and, possibly, on the fine details and anisotropy of the mechanical properties. In this respect, **Figure 5** shows the microstructures and the {111} pole figures of the 70% rolled samples, taking RD and ND as the reference axes. The rolled microstructures show high-angle grain boundaries (HAGBs), and one of the {111} slip planes aligned with the rolling direction; the broad bands are subdivided predominantly by low-angle grain boundaries (LAGBs). For the Cu and F138 samples, macroscopic shear bands appeared as dark-etched, narrow, and wavy bands aligned at approximately 55° to the loading direction. The shear bands are more conspicuous for the steel, which is the material with the lowest SFE. El-Danaf et al.[38] have reported that shear banding occurs much faster and becomes extensive even for early strain levels as the SFE is decreased, and this is the primary cause of modification of the main texture components. The same tendency is observed in the present results. All three materials developed a cellular LAGB structure, as shown in the boundary maps (Figure 5c,h).

Figure 6 shows the microstructures and the {111} pole figures for all three materials after a single ECAP pass, during which deformation is primarily by shear along a plane bisecting the channel angle. New HAGBs tend to form parallel to said plane, and in each grain, one of the {111} planes is aligned with ED. Deformation twin lines are more evident in the ECAP-processed samples, but Cu shows twinning activity only in some grains, whereas in the F138 steel, this deformation mechanism was very intense. When twinning is active, the initial grain is divided in twin lamellae, and further fragmentation occurs either by formation of dislocation cells inside the lamellae or by the formation of shear bands and twin intersections. Lamellae are ≈10 nm thick (see the TEM image in Figure 3), but at optical or SEM resolution, they appear as straight lines. For EBSD, the technique lacks resolution to distinguish twins from LAGB, and the lines are identified as the latter.

Different strain paths can be compared in terms of monotonicity, a parameter that expresses the uniformity of a deformation. According to Smirnov-Aljajev,[39] the two necessary conditions for a monotonic deformation are that 1) the relative state of the material lines and eigenvectors of the rate of deformation tensor do not change during the process; and 2) the triaxiality of the stress state remains constant (Lode parameter). The monotonicity is also reflected on the texture intensity, and

Table 3. Fitting parameters for Equation 1 according to ref.[20]]

Material	σ_0[MPa]	σ_1[MPa]	ε_c	n
AA1050	45	115	0.79	0.69
Cu	50	330	0.17	0.86
AISI 316L	300	1150	0.7	0.8

**ADVANCED
SCIENCE NEWS**

www.advancedsciencenews.com

*ADVANCED
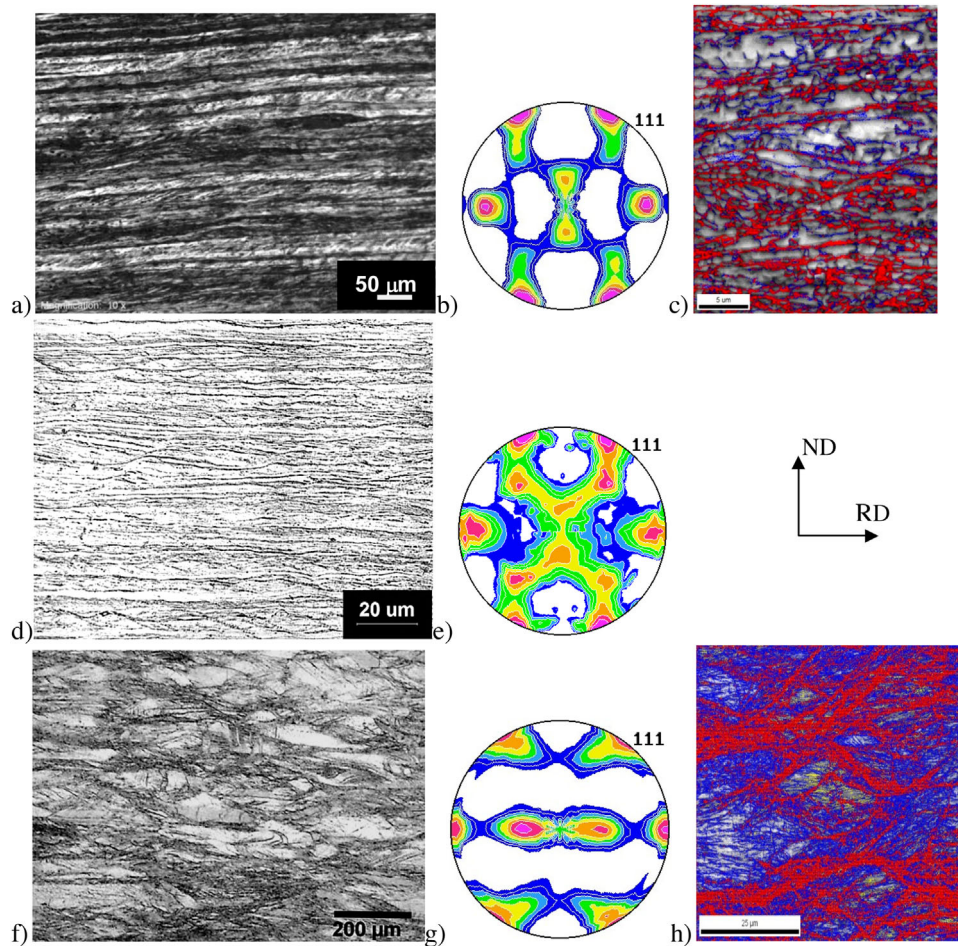ENGINEERING
MATERIALS*

www.aem-journal.com

Figure 5. Optical micrographs, {111} pole figures for the ND-RD plane and EBSD boundary maps (HAGB in red and LAGBs in blue) for the rolled samples: Al a–c), Cu d, e), and F138 f–h).

accordingly, ECAP processing shows a tendency to reduce the texture intensity,[40] whereas deformation by rolling tends to strengthen it.[41] In this respect, **Figure 7** compares the maximum intensity obtained in the {111} pole figures of the studied samples; both Cu and F138 follow the same tendency observed in a previous publication centered on Al.[42]

In an attempt to show the influence of deformation monotonicity on grain refinement, Bobor and Kralics[43,44] demonstrated that ECAP and torsion differ from a monotonic deformation and argue that this condition results in more efficient grain refinement. This is because ECAP is characterized by a complex mode of deformation consisting of shear, tension, and compression components; hence, the deformation path is non-stationary, a mode that enhances the deformation distribution (activates more and changing slip systems) while decreasing texture as deformation increases. In contrast, the rolling process is highly monotonic: in the plate half thickness, deformation by normal compression predominates rather than shear.

Figure 8 compares the effect of ECAP plus rolling ($\varepsilon_{eq} = 4.7$) and ECAP ($\varepsilon_{eq} = 4.0$) on the Al sample. For a similar amount of accumulated strain, a lower fraction of HAGBs was observed in the former group of samples when compared with the latter; its

microstructure consisted of subgrains or grains having similar crystallographic orientation, whereas in the ECAP sample, the orientation is less textured. From the boundary maps of Figure 8, it can be seen that the main difference between rolling and ECAP resides in the texture and the spatial distribution of the crystallographic components. Similar results were obtained by El-Danaf et al.[45] as well as on AA1050 Al after ECAP and plane strain compression, employing EBSD measurements on the TD-ND plane. Working with Cu, Jiang et al.[2] found that rolling after ECAP also increased texture and generated an aligned structure with a high fraction of HAGBs with its proportion increasing with ε_{eq}.

A modified Williamson-Hall (W-H) method was used to estimate grain sizes and dislocation densities. Planar defects such as twins or stacking faults were considered (the β Wg term in Eq. 1) only for the steel. The same contrast factors obtained by Ungár et al.[6–9] were employed in the calculations for the Cu and Al samples, while for the steel, the values for C_{11}, C_{12}, and C_{44} taken from steels with similar compositions were used to approximate the Wg constant (**Table 4**).[46]

In the W-H plots, the slope of the fitting curve is proportional to the square root of the dislocation density, whereas its
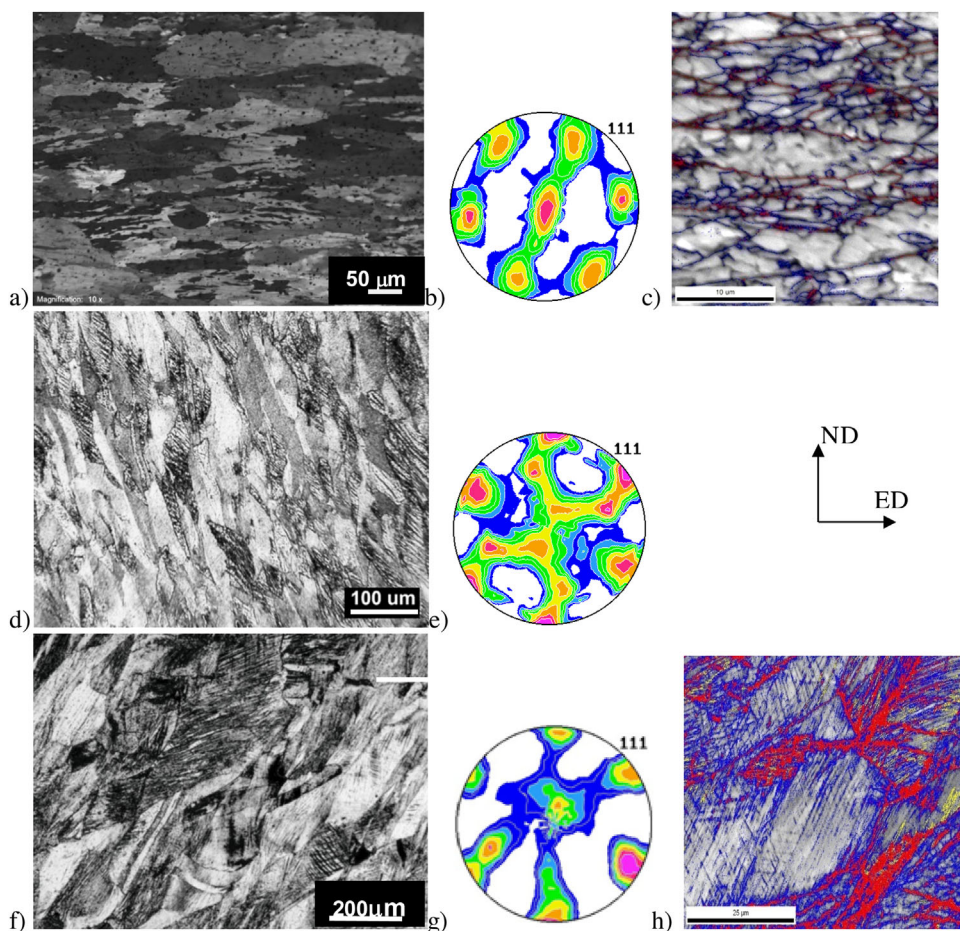
**ADVANCED
SCIENCE NEWS**

www.advancedsciencenews.com

**ADVANCED
ENGINEERING
MATERIALS**

www.aem-journal.com

Figure 6. Optical micrographs, {111} pole figures for the ND-ED plane, and EBSD boundary maps (HAGB in red and LAGBs in blue) for the samples after one ECAP pass: Al a–c), Cu d, e), and F138 (f–h).

intersection with the ΔK axis is proportional to the domain size. Said construction is shown in **Figure 9**, and data on domain size and dislocation density are summarized in **Table 5**, from which it can be seen that, upon decreasing the SFE of the analyzed material, the domain size decreases and the dislocation density increases. Quantitatively, these features are of the same order of magnitude for ECAP and for rolling, and in both cases increasing the equivalent strain increases the dislocation density and reduces the domain size. For the same strain level, however, rolling yields smaller domain sizes than route A ECAP, and this difference is more accentuated for Cu and F138.

For the steel, peak breadth analysis was performed for the three orthogonal reference planes, and the number of twins was also quantified for ECAP-processed (E) and rolled (R) samples (see **Figure 10**). The twin density in the latter sample was much lower than in the ECAP, in which these features were first activated parallel to the shear direction, and the transverse plane is the one that exhibits a higher proportion of twins after a single pass (see Figure 10a,b). For large strains, secondary twinning could also be observed in the normal and pressing planes. Furthermore, in these same ECAP samples, the dislocation density is higher in the pressing plane, where the twin density is lower, showing the complementary behavior of these

mechanisms. For the rolled sample, the dislocations are better distributed in all three orthogonal planes than when route A ECAP deformation is considered. Additionally, its mean density is higher than for the ECAP sample of same equivalent strain. Deformation twinning is sensitive to deformation rate and
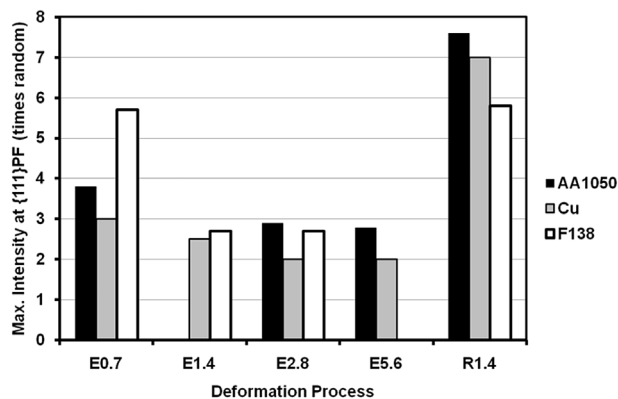

Figure 7. Intensity maximum values for the {111} pole figures for Al, Cu, and F138 steel.
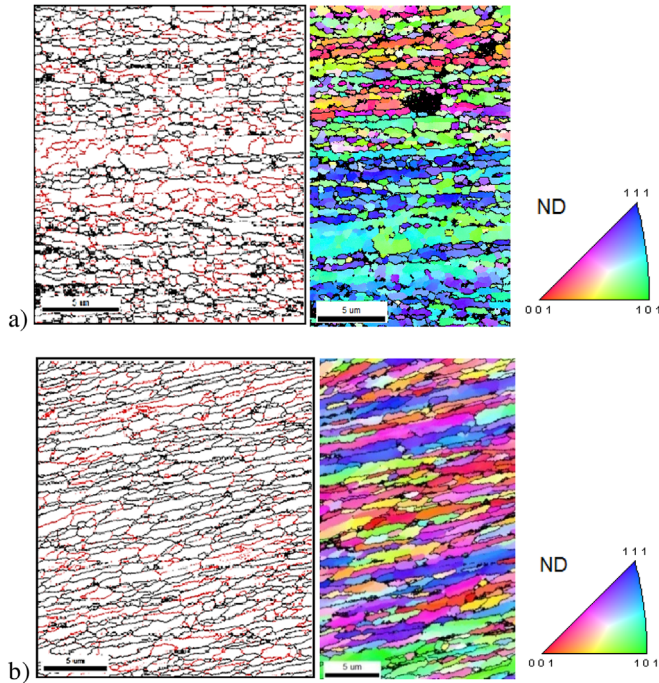
Figure 8. Boundary maps (HAGBs in black and LAGBs in red) and IPF maps for the Al samples: a) ECAP followed by rolling up to a von Mises strain of 4.2; b) only ECAP up to a von Mises strain of 5.6.

temperature,[47] and in ECAP, deformation is localized at the intersection plane of the channels, whereas for achieving the same accumulated strain, several rolling passes are necessary, meaning that deformation by ECAP is faster and proceeds in a much more localized way than that by rolling. Thus, another difference between ECAP and rolling is that materials with higher strain rate sensitivity and lower SFE may activate different deformation mechanisms in each process for the same strain level.

Twins and dislocation arrays will partition the grains in small domain areas, and Figure 10c shows that ECAP samples deformed to ε_{eq} equal 1.4 and 2.8; said domains are almost equal in the three orthogonal planes, that is, they are more spherical than in the rolled sample, where they are elongated in the rolling and transverse planes. Furthermore, rolling exhibits diffraction domains equal to or smaller than those of ECAP-processed samples.

4. Conclusions

Employing SPD processing, material yield strength can be enhanced up to a level corresponding to the establishment of an

Table 4. Elastic constants used for the modified W–H method.[6–9]

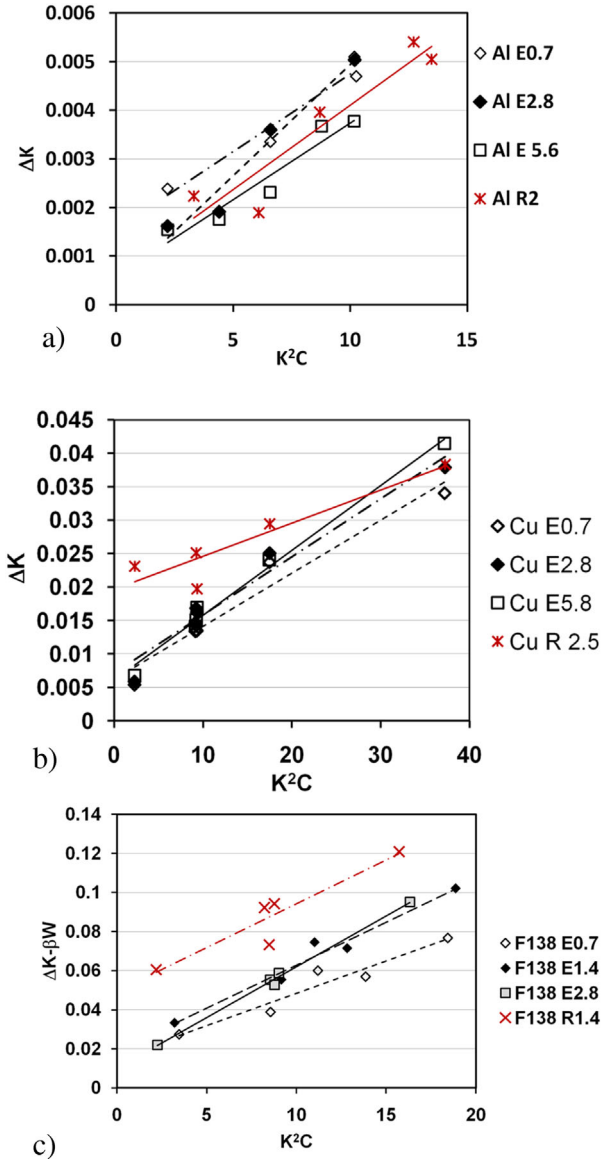|	C_{11}	C_{12}	C_{44}	A	C12/C44	Cav screw	Cav edge	q	M
AA1050	108	61	29	1.23	2.10	0.17	0.18	1.0	1
Copper	166	120	75.6	3.3	1.5	0.304	0.29	2.02	0.6
AISI 316	204	133	126	3.55	1.05	0.32	0.30	2.2	0.4

Figure 9. Modified W–H plots for ECAP (E) and rolling (R) at different equivalent strain levels: a) Al, b) Cu, and d) F138 Steel.

equilibrium domain size. Regardless of the deformation mode, this steady state corresponds to a von Mises strain of 3–4.

Although the stress–strain behavior is fairly well represented by a Voce-type flow equation, the deformation paths are different for each deformation mode, ECAP or rolling, and this has important consequences on the microstructure and, possibly, on the fine details and on the anisotropy of the mechanical properties.

The main difference between deformation by ECAP and by rolling comes from the different monotonicities of the strain paths and is reflected in the texture intensity.

Decreasing the SFE of the analyzed material, the domain size decreases and the dislocation density increases.

For an identical level of accumulated strain, a lower fraction of HAGBs was observed in the rolled samples when compared with

ADVANCED
SCIENCE NEWS
www.advancedsciencenews.com

ADVANCED
ENGINEERING
MATERIALS
www.aem-journal.com

Table 5. Results obtained from the modified W–H plots: Domain size (*D*) and dislocation density (ρ) for ECAP (*E*) and rolled (*R*) Samples.
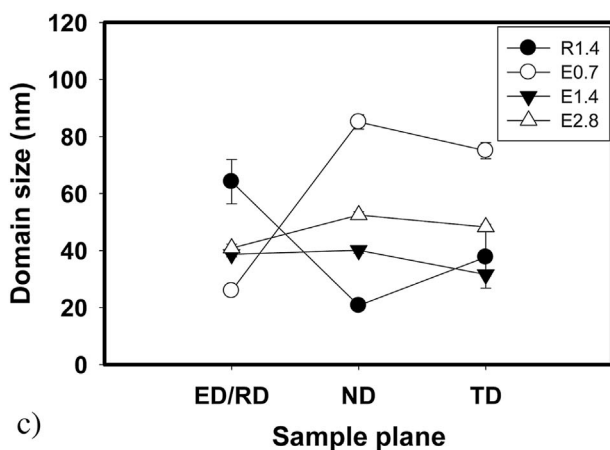
	AA1050				Cu				F138			
Process/strain	E0.7	E2.4	E5.8	R2.0	E0.7	E2.4	E5.8	R2.5	E0.7	E1.4	E2.8	R1.4
D (nm)	1190	2410	1551	1410	140	99	128	45	59	48	89	18
$\rho \times 10^{13}$ (m^{-2})	0.74	1.26	0.59	0.72	51	79	70	18	2170	2820	3960	2940
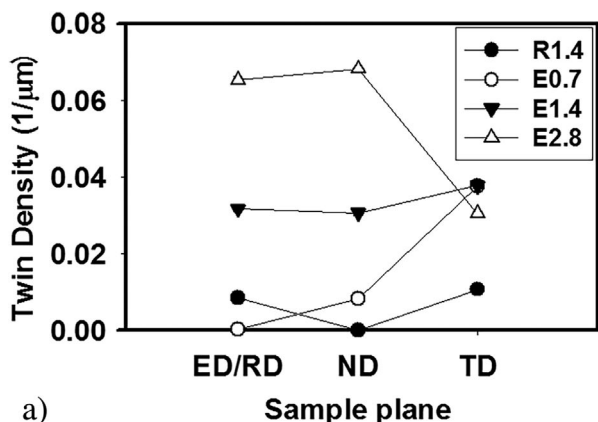
a)
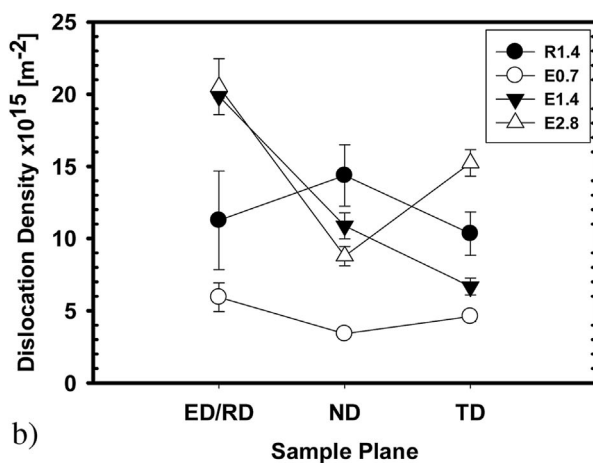
b)

c)

Figure 10. Values for twin density a), dislocation density b), and domain size c) measured in three orthogonal planes of the F138 samples. Numbers indicate the equivalent deformation level.

that of the ECAP samples. Furthermore, the microstructure consists of subgrains or grains of similar crystallographic orientation, whereas in the ECAP sample, the orientation is more random.

Another difference between ECAP and rolling is that materials with higher strain rate sensitivity and lower SFE may activate different deformation mechanisms in each process regardless of the strain level; thus, grain fragmentation by deformation-induced twins is more effective in ECAP.

When rolling is compared to ECAP, the former produces small diffraction domains, almost the same size or smaller than for ECAP processing, but ECAP domains were more spherical than those observed in the rolled sample.

Conflict of Interest

The authors declare no conflict of interest.

[1] Y. G. Ko, S. Namgung, B. U. Lee, D. H. Shin, *J. Alloys Compd.* **2010**, *504S*, 448.
[2] Y. Jiang, R. Zhu, J. T. Wang, Z. S. You, *J. Mater. Sci.* **2016**, *51*, 5609.
[3] Z. Horita, T. Fujinami, M. Nemoto, T. Langdon, *J. Mater. Process. Technol.* **2001**, *117*, 288.
[4] V. S. Sarma, J. Wang, W. Jian, A. Kauffmann, H. Conrad, J. Freudenberger, Y. Zhu, *Mater. Sci. Eng. A* **2010**, *527*, 7624.
[5] B. E. Warren, *Prog. Met. Phys.* **1959**, *8*, 147.
[6] T. Ungár, A. Borbély, *Appl. Phys. Lett.* **1996**, *69*, 3173.
[7] T. Ungár, I. Dragomir, A. Revesz, A. Borbély, *J. Appl. Crystallogr.* **1999**, *32*, 992.
[8] I. C. Dragomir, T. Ungár, *J. Appl. Crystallogr.* **2002**, *35*, 556.
[9] G. Ribárik, T. Ungár, J. Gubicza, *J. Appl. Crystallogr.* **2001**, *34*, 669.
[10] G. Caglioti, A. Paoletti, F. Ricci, *Nucl. Instrum. Methods* **1958**, *3*, 223.
[11] G. K. Williamson, W. H. Hall, *Acta Metall.* **1953**, *1*, 22.
[12] T. Ungar, J. Gubicza, G. Ribarik, A. Borbely, *J. Appl. Crystallogr.* **2001**, *34*, 298.

ADVANCED
SCIENCE NEWS

www.advancedsciencenews.com

ADVANCED
ENGINEERING
MATERIALS

www.aem-journal.com

[13] G. T. Gray, *Annu. Rev. Mater. Res.* **2012**, *42*, 285.

[14] E. El-Danaf, S. R. Kalidindi, R. D. Doherty, *Metall. Mater. Trans. A* **1999**, *30*, 1223.

[15] D. R. Steinmetz, T. Jäpel, B. Wietbrock, P. Eisenlohr, I. Gutierrez-Urrutia, A. Saeed-Akbari, T. Hickel, F. Roters, D. Raabe, *Acta Mater.* **2013**, *61*, 494.

[16] G. B. Olson, M. Cohen, *Metall. Trans. A* **1976**, *7*, 1897.

[17] S. Allain, J. P. Chateau, O. Bouaziz, *Mater. Sci. Eng. A* **2004**, *387*, 143.

[18] S. Gao, M. Chen, S. Chen, N. Kamikawa, A. Shibata, N. Tsuji, *Mater. Trans.* **2014**, *55*, 73.

[19] X. G. Qiao, N. Gao, M. J. Starink, *Philos. Mag.* **2012**, *92*, 446.

[20] N. Q. Chinh, G. Horváth, Z. Horita, T. G. Langdon, *Acta Mater.* **2004**, *52*, 3555.

[21] V. Szombathelyi, G. Krallics, *IOP Conf. Ser.: Mater. Sci. Eng.* **2014**, *63*, 12051.

[22] T. Csanádi, N. Q. Chinh, J. Gubicza, T. G. Langdon, *Acta Mater.* **2011**, *59*, 2385.

[23] M. A. Abdulstaar, M. Mhaede, M. Wollmann, L. Wagner, *J. Mater. Sci.* **2014**, *49*, 1138.

[24] S. X. Zhou, J. Zhong, D. Mao, M. P. Funke, *J. Mater. Process. Technol.* **2003**, *134*, 363.

[25] J. Zhang, N. Gao, M. J. Starink, *Mater. Sci. Eng. A* **2011**, *528*, 2581.

[26] B. Leszczynska-Madej, P. Pałka, M. Richert, *Arch. Metall. Mater.* **2014**, *59*, 313.

[27] L. Su, C. Lun, H. Li, G. Deng, K. Tieu, *Mater. Sci. Eng. A* **2014**, *614*, 148.

[28] G. Purcek, O. Saray, M. I. Nagimov, A. A. Nazarov, I. M. Safarov, V. N. Danilenko, O. R. Valiakhmetov, R. R. Mulyukov, *Philos. Mag.* **2012**, *92*, 690.

[29] T. G. De Sousa, *Avaliação de Densidade de Discordâncias em Cobre e Latão α Deformados por Análise de Largura de Pico de drx*, Instituto Militar de Engenharia, Dissertação, Rio de Janeiro **2012**.

[30] D. Orlov, A. Vinogradov, *Mater. Sci. Eng. A* **2011**, *530*, 174.

[31] T. Sakai, H. Miura, X. Yang, *Mater. Sci. Eng. A* **2009**, *499*, 2.

[32] N. Nagashima, S. Matsuoka, *Mater. Trans.* **2006**, *47*, 2326.

[33] J. Przondziono, D. Halaczek, J. Szymszal, *Arch. Civ. Mech. Eng.* **2007**, *7*, 85.

[34] P. Czarkowski, A. Krawczynska, R. Slesinski, T. Brynk, J. Budniak, M. Lewandowska, K. Kurzydlowski, *Fusion Eng. Des.* **2011**, *86*, 2517.

[35] M. Greger, L. Kander, R. Kocich, *Arch. Mater. Sci. Eng.* **2008**, *31*, 41.

[36] Y. Nakao, H. Miura, *Mater. Sci. Eng. A* **2011**, *528*, 1310.

[37] H. Ueno, K. Kakihata, Y. Kaneko, S. Hashimoto, A. Vinogradov, *J. Mater. Sci.* **2011**, *46*, 4276.

[38] E. A. El-Danaf, A. Al-Mutlaq, M. S. Soliman, *Mater. Sci. Eng. A* **2011**, *528*, 7579.

[39] G. A. Smirnov-Aljaev, *Soprotivlenie Materialov Plasticheskomu Defformirovaniju*, Mashinoctroenie, Leningrad, Russland **1978**, p. 368.

[40] P. W. J. Mckenzie, R. Lapovok, *Acta Mater.* **2010**, *58*, 3212.

[41] O. Mishin, A. Godfrey, D. J. Jensen, N. Hansen, *Acta Mater.* **2013**, *61*, 5354.

[42] M. C. V. Vega, R. E. Bolmaro, M. Ferrante, V. L. Sordi, A. M. Kliauga, *Mater. Sci. Eng. A* **2015**, *646*, 154.

[43] K. Bobor, G. Krallics, *Rev. Adv. Mater. Sci.* **2010**, *25*, 32.

[44] K. Bobor, G. Krallics, *J. Phys.: Conf. Ser.* **2010**, *240*, 012126.

[45] E. A. El-Danaf, M. S. Soliman, A. A. Almajd, *J. Mater. Sci.* **2011**, *46*, 3291.

[46] R. W. Smith, G. S. Was, *Phys. Rev. B* **1989**, *40*, 10322.

[47] Y. Zhang, N. R. Tao, K. Lu, *Acta Mater.* **2011**, *59*, 6048.

1700055 (10 of 10)